REPORT DOCUMENTATION PAGE

AFRL-SR-AR-TR-03-

0207

ublic reporting burden for this collection of information is estimated to average 1 hour per response, including the time for reviewing instructions,
ed, and completing and reviewing this collection of information. Send comments regarding this burden estimate or any other aspect of this collec
ient of Defense, Washington Headquarters Services, Directorate for Information Operations and Reports (0704-0188), 1215 Jefferson Davis Hig.
hat notwithstanding any other provision of law, no person shall be subject to any penalty for failing to comply with a collection of information if it does not display a cui...
IETURN YOUR FORM TO THE ABOVE ADDRESS.

. REPORT DATE (DD-MM-YYYY) 4-01-2003	2. REPORT TYPE Final Performance	3. DATES COVERED (From - To) 01-12-1999 to 30-11-2002
. TITLE AND SUBTITLE hase Stability and Microstructure Control in High Temperature (Mo,Nb)-Si-B Alloys		5a. CONTRACT NUMBER
		5b. GRANT NUMBER F49620-00-1-0077
		5c. PROGRAM ELEMENT NUMBER
. AUTHOR(S) rofessor John H. Perepezko		5d. PROJECT NUMBER
		5e. TASK NUMBER
		5f. WORK UNIT NUMBER
PERFORMING ORGANIZATION NAME(S) AND ADDRESS(ES) niversity of Wisconsin-Madison esearch Administration 50 University Ave. adison, WI 53706		8. PERFORMING ORGANIZATION REPORT NUMBER
SPONSORING / MONITORING AGENCY NAME(S) AND ADDRESS(ES) F Office of Scientific Research esearch/NA (Dr. C. Hartley) 01 N. Randolph Street rlington, VA 22203		10. SPONSOR/MONITOR'S ACRONYM(S)
		11. SPONSOR/MONITOR'S REPORT NUMBER(S)

. SUPPLEMENTARY NOTES

. ABSTRACT

high temperature (T>1400°C) environment imposes severe constraints on materials selection in terms of melting temperature, oxidation resistance and ructural functionality. Multiphase microstructure designs in the Mo-Si-B system, involving a ternary intermetallic Mo_5SiB_2 (T_2) phase as a critical nstituent, have been identified that offer the attractive potential to satisfy the challenging requirements. An inherent phase stability in the Mo-Si-B system is been established at 1600°C, a sluggish diffusion that is critical in achieving robust multiphase microstructures, limiting oxidation and minimizing creep is been confirmed, and a unique precipitation has been discovered to contribute to strengthening and toughening. From a foundation of the established iase equilibrium in the Mo-Si-B system at 1600°C a systematic examination has been initiated into the phase stability and solidification pathways that nstitute essential factors in developing a control of the microstructural evolution. The T_2 phase is clearly a key member of any alloy design since it velops equilibria with each of the binary boride and silicide phases for Mo-rich alloys in the Mo-Si-B system. The T_2 phase shows a compositional istence range so that constitutional defects are critical to understanding the stability. Analysis of the T_2 phase growth kinetics yields diffusivities of about r^{16} m^2/s at 1600°C. Following solidification processing Mo-Si-B alloys exhibit extensive segregation in the form of non-equilibrium phases. . Alternate ocessing by rapid solidification or selected alloying such as partial substitution of Mo by Nb or W has been demonstrated to effectively reduce segregation yield two phase ($Mo_{ss}+T_2$) and a new three-phase ($RM+T_1+T_2$) microstructures directly during solidification. The structural modification due to alloying veals the central role that the atomic sizes and the constitutional defect structure play in the structural stability of the T_2 phase. The current understanding ovides effective guidance to optimize new multiphase designs and processing.

. SUBJECT TERMS
.gh Temperature Alloys, Refractory Metals, Phase Stability, Diffusion, Multiphase Microstructure

. SECURITY CLASSIFICATION OF:			17. LIMITATION OF ABSTRACT	18. NUMBER OF PAGES	19a. NAME OF RESPONSIBLE PERSON
REPORT	b. ABSTRACT	c. THIS PAGE		31	19b. TELEPHONE NUMBER (include area code)

20030618 123

TABLE OF CONTENTS

1. Introduction

The challenges of a high temperature environment (T>1400°C) impose severe material performance constraints in terms of melting point, oxidation resistance and structural functionality. A number of ceramic materials, intermetallic compounds and refractory metals with high melting temperature are available as material choices. However, in a single component, single phase form, these materials rarely satisfy all the above requirements because of the brittleness of ceramic materials and intermetallic compounds at low temperatures and the oxidation problems and poor creep resistance of refractory metals at high temperatures. In this respect the evolutionary development of high temperature alloys over the past 4-5 decades represents a remarkable achievement and provides important lessons to guide future materials design efforts. One clear message is the importance of multiphase microstructures and the capability to control phase fractions and morphologies within the overall structure [87Sto,87Ros,90Dys]. The flexibility in microstructure control has been shown to be critical in tailoring alloy performance in order to satisfy a number of mechanical property requirements that sometimes present conflicting demands [92Dim,91Kim]. Besides the essential structural requirements, elevated temperatures also often involve aggressive environments that require a material to display an inherent oxidation protection that can be enhanced further by coating [79Mai].

In terms of metallic system candidates there are several high melting temperature intermetallics, but there is a much smaller number of intermetallic phases that offer a level of inherent environmental resistance. At elevated temperature, alloy phases that contain Al or Si are most attractive for developing stable Al_2O_3 and SiO_2 coatings. Moreover, above about 1300°C, SiO_2 films are preferred since the parabolic rate constant for oxidation is lower for SiO_2 than for Al_2O_3 [83Bir]. In fact, this selection is supported by the superior oxidation resistance available with monolithic $MoSi_2$ where a SiO_2 surface provides for useful operation up to about 1700°C (i.e. $0.8 T_m$). At high temperatures the creep strength of $MoSi_2$ is insufficient and at low temperature it is brittle [92Vas,92Sha,92Boe].

At the same time, the multiphase microstructures that can be developed in the Mo-Si-B system involving the high melting temperature (>2100°C) ternary-based intermetallic Mo_5SiB_2 (T_2) offer an attractive option particularly due to the superior oxidation resistance of the Mo-based silicides [97Per,97Nun]. In terms of the available phase combinations in the Mo-Si-B system, the two-phase combination of Mo(ss) +T_2 offers enhanced toughening [00Nun] due to a precipitation of Mo(ss) that can be produced within the T_2 phase [98Sak,99Sak-a,99Sch] while three phase alloys comprised of Mo(ss), T_2 and Mo_3Si or Mo_3Si, T_2 and Mo_5Si_3 offer favorable oxidation resistance [99Sch,98Sch,93Tho]. A focal point of the microstructural designs is clearly the T_2 phase that is central to the phase selections that promote high temperature stability and robust microstructures. In this regard, a comprehensive assessment of the solidification behavior is critical as well since the solidification structure ultimately plays a key role in the morphological control of the microstructure. The T_2 phase develops upon solidification through a peritectic reaction and exhibits a range of solubility [00Nun]. Consequently, constitutional defects must be introduced to accommodate non-stoichiometric compositions. In ternary alloys direct formation of Mo+T_2 structures is not possible due to severe segregation under usual solidification processing conditions [99Sak-b]. Rapid solidification processing such that available in powders is effective in suppressing the solidification segregation [97Per,99Sak-b]. However, alternate approaches are also of interest for bulk ingots. For example, selected refractory metal substitutional alloying, such as the incorporation of Nb to alter the solubility of the T_2 phase and the relative

phase stability has been shown to be an effective method to control the solidification of two phase refractory solid solution + T_2 structures [00Sak]. The observed alloying trends also highlight the fundamental factors related to the defect structure and atomic size factor that influence the relative stability of the T_2 phase and provide a basis to develop a thermodynamic model of the phase equilibria. Coupled with the thermodynamic predictions, the synergy of phase stability and solidification control will be a critical prerequisite for further microstructure developments.

It is appropriate to consider briefly some of the contemporary approaches to developing phase stability models in complex multicomponent multiphase systems. Indeed this major task has been a challenge for some time. However, a variety of approaches have evolved that have made useful contributions to the understanding in simpler systems, but also reveal some limitations. For example, electronic structure calculations have been advanced by the use of density-functional theory (DFT) as a many-body approach and the application of the local density approximation (LDA). By simplifying the DFT problem to treat valence electrons under the assumption that the core electrons experience little change due to the chemical reactions, further advancement has been achieved by the introduction of the plane-wave pseudopotential (PW-PP) technique [00Alf]. This approach has enabled the band structures as well as other physical properties of the transition metals, in particular, to be elucidated. Moreover, the use of Debye model which incorporates the phonon contribution to the elastic response has been successful in examining refractory silicides that typically exhibit a strong p-d hybridization with correspondingly high optical phonon energies. Fu et. al. for example have been able to analyze the thermoelastic characteristics of the refractory silicides including the T_2 and T_1 phases and pointed to the source of the large coefficient of thermal expansion (CTE) anisotropy in the T_1 phase as due to a high lattice anharmonicity in the <001> direction and a elastically stiff basal plane [00Fu]. Furthermore, the calculation is also consistent with the more isotropic behavior of the CTE in the T_2 phase since the short Mo-Mo chains in the T_1 phase are not present in the T_2 phase. Overall, the first principle types of calculations give useful estimates of the ground state behavior and the low temperature relative phase stability. In fact, the calculated energies for different stoichiometric reference structures are often in reasonable agreement with the lattice stabilities evaluated by thermodynamic analysis [00Alf]. However, a complete description of the relative phase stability over a wide range of temperature and composition with the inclusion of constitutional defects and phase transitions remains a challenge and a limitation to providing the necessary guidance for effective multiphase designs in structural applications.

At the same time, when considering a system for the first time, it is necessary to have a baseline of phase stability knowledge before attempting any model development. In fact, as the database grows, the level of modeling can also evolve, but an initial effort can offer significant benefit if it maintains a contact with the database in order to minimize the number of limiting assumptions. For this purpose, a computational thermodynamic model in the spirit of the CALPHAD approach is proposed since it provides an effective basis for the interpolation of results as well as for the extrapolation of behavior outside of the database to give predictive guidance.

The central theme in this proposal is to coordinate a comprehensive approach involving joint experimental and modeling work that integrates multiphase stability concepts and models to provide insight into the control of solidification and multiphase reactions to guide the design of high temperature T_2-based microstructures and alloy compositions. The examination of multiphase stability centering on the T_2 phase will incorporate a careful

determination of the defect structure mechanisms that control the phase stability. TEM studies will provide an analysis of dislocation structures. Similarly, a parallel effort will be devoted to examine the changes in T_2 phase stability with refractory metal and metalloid substitution. These critical experimental observations will enable the formulation of a comprehensive thermodynamic modeling of the stability of the T_2 phase as well as the multiphase configurations involving the T_2 phase.

2. Research Highlights

2.1. Phase Stability in the Mo-Si-B System and Defect Structures in the T_2 Phase

Based upon the EPMA examination [00Fou] of phase compositions in the long-term annealed samples and x-ray diffraction determination of phase identity, the Mo-rich portion of the phase diagram isotherm for the Mo-Si-B system at 1600°C has been established as shown in Figure 1. In the present study that is supported by the AFOSR, the main emphasis is on the phase equilibrium bordered by the Mo-MoB-Mo_5Si_3 region. Within this region the central role of the T_2 phase as a key constituent is the phase stability is evident. Recently, the Mo-rich phase diagram isotherm for the Mo-Si-B system at 1600°C has been extended to the Mo-MoB-$MoSi_2$ region. The EPMA examination on 3-phase equilibrium (MoB, Mo_5Si_3 and $MoSi_2$) samples provided the phase boundary composition information. The homogeneity region of the boride phases (Mo_2B and MoB) at 1600°C in general indicates a very small Si solubility (less than 0.25 at. %). The Mo(ss) phase has a negligible B solubility, but appreciable Si solubility up to about 3 at% Si. The Mo_3Si phase has a limited homogeneity region that ranges from about 24 to 25 at. % Si and a negligible B solubility [00Ros]. The compositional boundary of Mo_5Si_3 (T_1 phase) on the Mo-rich side extends to ~37 at% Si and on the Si-rich side to ~39 at% Si. The B solubility in the T_1 phase has been found to be much more limited than that reported by Nowotny [57Now] and is in agreement with a recent assessment [00Hue].

The homogeneity range of the T_2 phase with the corresponding change in the lattice constants is given in Table 1. The effect of B/Si ratio on the monotonic variation in the cell volume is evident. The compositional variation in the T_2 phase with respect to the B/Si ratio in the off-stoichiometric region is mostly towards B-rich values which is indicated with B/Si ratio values greater than 2.0. This is consistent with a prior analysis on the stability of the T_2 phase which points to the relative ease in B to Si anti-site substitution, but not Si to B anti-site substitution

The apparent operation of anti-site B-Si substitution over a portion of the stability range is consistent with the observations from other ternary systems that exhibit the ternary-based T_2 phase. In fact, in the Nb-Si-B system (Figure 1c) for instance it is possible to accommodate a large solid solution mixing of the metalloid constituents in the T_2 phase as manifested by the wide span of B and Si homogeneity range. It is worth noting here that while a large degree of mixing in the metal sublattice is common for the metal-rich silicides phases, only the T_2 phase appears to display also a large degree of metalloid mixing.

In addition to the anti-site substitution defect mechanism, there appears to be a different defect structure that influences the temperature dependence of Mo solubility in the T_2 phase. The formation of the Mo(ss) precipitates in

Table 1 Lattice parameter measurements as functions of composition for the T_2 phase.

Phase equilibrium	B/Si ratio in T_2	Mo at. % in T_2	a (nm)	c (nm)	c/a	a^2c (nm)^3
T_2 + Mo_2B + MoB	2.913	63.06	0.6005	1.1056	1.841	0.3987
T_2 + Mo_2B + Mo(ss)	2.177	64.10	0.6026	1.1080	1.839	0.4023
T_2 + Mo_3Si + Mo(ss)	1.992	63.65	0.6029	1.1095	1.840	0.4033
T_2 + Mo_3Si + Mo_5Si_3	1.917	61.20	0.6061	1.1136	1.837	0.4091

the T_2 primary phase (see Figure 2) suggests that there is an additional role of a vacancy-based defect structure that both promotes the precipitation process and determines the magnitude of the Mo solubility limit variation with temperature.

2.2. Stability of the T_2 Crystal Structure

For a further examination on the stability of the T_2 phase, it is useful to observe the crystal structure at the stoichiometric composition. The Mo_5SiB_2 phase has the $D8_1$ structure which has a body-centered tetragonal unit cell (space group I4/mcm) as shown in Figure 3. The unit cell contains 32 atoms which means 20 Mo, 4 Si and 8 B atoms are situated in layered arrangements. Three types of layers can be identified: layer A with only Mo atoms, layer B with only Si atoms and layer C with a mixture of Mo and B atoms. The structural arrangement of these layers in T_2 has been viewed as the means to achieve an efficient atomic packing between metal atoms such as Mo and metalloid constituents (Si and B in this case) [58Aro,84Fra]. Based on the radius ratio of the metal atom and the metalloid atoms, variations in the successive stacking can be constructed. The relatively large difference in atomic radius of the two types of metalloids necessitates stacking arrangements of the A layers that would yield two distinct sites. Layer arrangements of A - A $_{1/2 1/2}$ - A $_{1/2 1/2}$ - A – A- in the [001] direction are therefore developed in the T_2 structure. The $A_{1/2 1/2}$ layer refers to the A layer that has been translated by half the base diagonal relative to neighboring layers. With the A-A $_{1/2 1/2}$ or A $_{1/2 1/2}$ –A arrangements, a cubic anti-prismatic site is created and filled by Si atoms forming the layer B (see Figure 3). The B atoms on the other hand are situated in the trigonal prismatic hole generated by sandwiching two symmetrically oriented A layers (the A-A or $A_{1/2 1/2}$ – $A_{1/2 1/2}$ layer arrangements). In this site, the B atoms are capped by two triangular arrangements of Mo atoms along the c axis and one B and two more Mo atoms forming an intermediate layer (layer C). The two Mo atoms fill the remaining available hole created by the A-A layer arrangements that accordingly constitutes the largest hole available (the cubic prismatic hole). Thus, the limited ability to stabilize the T_2 phase in the Si-rich region in the Mo-Si-B system may be interpreted as the difficulty in situating Si atoms in the B sub-lattice in the trigonal prismatic hole. On the other hand, there is a ready accommodation of B atoms in the Si lattice position which is also indicated by the reduction of the cell volume for B-rich T_2 compositions. The limitation in the enriching the T_2 phase with Si appears to be related to the limited available volume of the B sublattice.

The implication of the preference of site occupancy between the metalloid constituents is that the T_2 phase non-stoichiometry in the Mo-Si-B system always occurs in the B-rich region. However, the fact that the stability of the T_2 crystal structure appears to be strongly affected by the atomic size ratio [84Fra,95And] may facilitate a greater modification in the mixing behavior of the metalloid constituents in their two sublattices. This is exemplified with the selected refractory metal substitution that is employed to alter the mixing proportion of the metalloid element. Furthermore, the metalloid compositional span can be dramatically enhanced by the use of selected alloying substitutions. It is important to point out that while the extended refractory metal alloying is typically observed in other metal-rich silicide or boride structures (e.g. $(Mo,RM)_5Si_3$, $(Mo,Ti)Si_3C$, $(Mo,Cr)_3Si,(Mo,W)_2B$, $(Mo,Cr)B$), none of these structure classes results in an expansion of the metalloid solubility as exemplified in Nb-Si-B ternary system. It seems that while the atomic size ratio influences the overall stability of the crystal structure, the existence

of a large compositional span in the metalloid contents also means that the normally rigid covalent bonding characteristics in the T_2 that are reflected in the nearly constant Mo-Si and Mo-B interatomic distances can be adequately compensated by the c/a variations. In the case of T_2 phase in the Nb-Si-B system, indeed a systematically monotonic change in the c/a with the B/Si ratio in the T_2 phase is observed.

The refinement on the lattice constants from a single crystal T_2 phase has been performed (the specimen was procured from Kyoto University, Japan as a part of collaborative work with Prof. Yamaguchi's research group). The structure was determined from direct methods (using SHELX crystal refinement program) and refined on F^2 (for 127 unique reflections Fo > 4sig(Fo) and for 16 independent parameters) to unweighted and weighted discrepancy factors of R(F)= 0.0332 and wR = 0.0748 respectively. Figure 3(d,e) shows selected slices of the Fourier map along the c axis that reflects the total electron density. The maps show the existence of directional covalent bonding between Mo-Mo atoms in addition to Mo-Si and Mo-B atomic bonding. Table 2 lists the four unique atomic positions in addition to both isotropic and anisotropic variable displacement (thermal) parameters. The relative atomic positions are in an agreement with the current refinement work from powder X-ray diffraction [01Raw]. Table 3 lists the relatively short interatomic distances in the T_2 phase which further support the presence of covalent bonding.

Table 2. *Refined fractional coordinates (x,y,z) and the displacement thermal paramaters (in $Å^2$) for the T_2 Phase at Room Temperature. (a = 6.0298 Å , c = 11.0760 Å)*

Atom	x	y	z	U11=U22	U33	Ueq
Mo1	0.00000	0.00000	0.00000	0.00178	0.00373	0.00243
Mo2	0.16487	0.66487	0.14046	0.00257	0.00364	0.00293
Si	0.00000	0.00000	0.25000	0.00434	0.01471	0.00779
B	0.38152	0.88152	0.00000	0.00318	0.00001	0.00212

Table 3. *The interatomic distances in the T_2 phase*

Atom1	Atom2	Shortest distance Å	Atom1	Atom2	Shortest distance Å
Mo1	B	2.4089	Mo2	Mo1	2.7372
Mo1	Si	2.7372	B	B	2.0207
Mo2	B	2.3276	B	Mo1	2.4089
Mo2	Si	2.5581			

2.3. Thermodynamic Evaluation of the Phase Equilibria

In order to provide a basis for the reliable analysis of the measured phase stability and to provide guidance in the further analysis and interpretation of the character of the defect structure in the T_2 phase an evaluation of the thermodynamic properties is necessary. Currently, reliable thermodynamic data for the T_2 phase are not available. However, either the limiting tangent method or the limiting reaction stability method that uses the data on the phases coexisting in equilibrium with the T_2 phase (Figure 1) can be applied to establish reasonable bounds on the free energy of formation of the T_2 phase. As a first level of analysis, all phases are treated as line phases without any mutual solubility. Next, the available thermodynamic information on the binary phases such as the free energy of formation, ΔG_f, is considered together with the established ternary phase equilibrium relationships. For the limiting tangent method, since the observed ternary phase equilibria yields the ($Mo_{ss} + Mo_2B + T_2$) and the ($Mo_{ss} + Mo_3Si +$

T_2) three phase fields, the ΔG_f for the T_2 phase is constrained so that the common tangent planes for the three phase fields noted preclude the establishment of a ($Mo_2B + Mo_3Si$) two-phase field [95Gas,92Kub]. In a similar manner, by comparing other possible competing phase equilibria with the observed phase relations, upper and lower bounds for ΔG_f for the T_2 phase can be established at 1600°C [95Gas,92Kub]. In order to establish an estimated ΔG_f for further analysis, a mean value is applied which is -130.9 ± 0.6 kJ/g-atom (or −1047.30 ± 5.29 kJ/mole). The same procedure can be repeated for different temperatures between 1200 to 1600 °C to estimate the temperature dependence of $\Delta G_f \cong$ -100.3 − 0.505T (kJ/mole).

For the limiting reaction stability, the phase stability diagram and thermodynamic reactions among borides, silicides and T_2 provide a critical condition that T_2 exists as a stable phase [95Gas,92Kub]. Four limiting thermodynamic reactions were used to calculate the Gibbs free energy for the T_2 phase as shown in Figure 4:

(1) $Mo_3Si + 2MoB = T_2$

(2) $6Mo_2B + Mo_5Si_3 (T_1) = 2Mo + 3T_2$

(3) $2Mo_2B + Mo_3Si = 2Mo + T_2$

(4) $7T_2 + 4MoSi_2 = 14MoB + 5Mo_5Si_3$

The phase stability diagram (Figure 1) indicates that Mo_3Si and MoB in reaction (1) are not in two-phase equilibrium and T_2 exists as a stable phase. In order for T_2 in reaction (1) to be stable, $(\Delta G_f(Mo_3Si) + 2 \Delta G_f(MoB)) > \Delta G_f(T_2)$. This relationship yields that −1011.11 (kJ/mol) $> \Delta G_f(T_2)$ at 1600 °C. In reaction (2), since Mo and T_2 are in two-phase equilibrium, $(6 \Delta G_f(Mo_2B) + \Delta G_f(Mo_5Si_3)) > (2 \Delta G_f(Mo) + 3 \Delta G_f(T_2))$. This relationship yields that − 1032.76 (kJ/mol) $> \Delta G_f(T_2)$ at 1600 °C. In reaction (3), since Mo and T_2 are in a two-phase equilibrium, $(2 \Delta G_f(Mo_2B) + \Delta G_f(Mo_3Si)) > (2 \Delta G_f(Mo) + \Delta G_f(T_2))$. This relationship yields that −1040.76 (kJ/mol) $> \Delta G_f(T_2)$ at 1600 °C. In reaction (4), since MoB and Mo5Si3 are in a two-phase equilibrium, $(7 \Delta G_f(T_2) + 4 \Delta G_f(MoSi_2)) > (14 \Delta G_f(MoB) + 5 \Delta G_f(Mo_5Si_3))$. This relationship yields that $\Delta G_f(T_2) > -1052.67$ (kJ/mol) at 1600 °C. Therefore, when −1052.67 (kJ/mol) $< \Delta G_f(T_2) < -1040.76$ (kJ/mol), all the above thermodynamic reactions move to equilibrium states that coincide with the phase stability diagram. Moreover, a mean value is applied to establish an estimated ΔG_f which is -130.84 ± 0.75 kJ/g-atom (or −1046.71 ± 5.96 kJ/mole). Because the bounding limits that are determined by both methods are relatively small (i.e. within a few per cent) the two approaches yield similar values of the Gibbs free energy for T_2.

The use of the estimated value for ΔG_f for the T_2 phase and the established ΔG_f values for the binary phases allows for the calculation of a self-consistent isotherm at 1600°C as shown in Figure 1b. The final result does demonstrate that the main features of the phase stability observed at 1600°C can be reproduced by the thermodynamic calculation. At the present stage there are also clear limitations on the calculation method since it treats phases as line compounds and employs an approximate value for ΔG_f for the T_2 phase. However, the approach illustrates the potential for a full analysis once measurements of the solubilities and analysis of the defect structures of the intermediate phases are used to develop solution models.

2.4. Assessment of the Diffusion Behavior Involving T_2 Phase Formation

A diffusion study is in progress to examine the formation of the T_2 phase as a diffusion reaction product between the Mo_2B and Mo_5Si_3 phases. Annealing the Mo_2B/Mo_5Si_3 diffusion couple yields the diffusion pathway of either $Mo_2B/T_2/Mo_5Si_3$ or $Mo_2B/T_2/Mo_3Si/Mo_5Si_3$. Figure 5 shows the back-scattered electron (BSE) image from the cross-section of the diffusion couple annealed at 1600°C for 100 hrs and reveals the diffusion pathway of $Mo_2B/T_2/Mo_3Si/Mo_5Si_3$, which indicates that the Mo_3Si phase initiates and grows from the Mo_5Si_3 phase. The interface between Mo_3Si and Mo_5Si_3 exhibits an irregular boundary. It is also evident that the Mo_5Si_3 phase in Figure 5(a) exhibits cracking that is absent in the Mo_3Si phase.

Figure 5(a) also shows that the T_2 phase initiates and grows from the Mo_2B phase. The interface between T_2 and Mo_2B macroscopically exhibits a planar interface, though the T_2 grains grow with a columnar structure, which is identified from TEM analysis (Figure 6). The grain boundary between the T_2 grains in Figure 6 was analyzed by the high resolution TEM (HRTEM). On the HRTEM image (Figure 7) the orientation of the (200) plane on the upper T_2 grain (white dashed line) is approximately in accord with that on the lower T_2 grain (white lines). In other words, two T_2 columnar grains have a low angle grain boundary. The electron diffraction pattern (Figure 8) on the T_2 grain indicates that the electron beam direction is [001] and normal to (001) plane. This indicates that there is a clear tendency for the growth of T_2 to be approximately normal to c-axis.

The diffusion pathway of $Mo_2B/T_2/Mo_3Si/Mo_5Si_3$ has been found also in diffusion couples annealed at 1600 °C for 200 and 500 hrs as well as at 1700 and 1800 °C. A plot of the diffusional growth kinetics for the T_2 phase based upon the initial results is given in Figure 9. Assuming that the initial thickness of the T_2 phase layer is negligible, the rate constant k was calculated by linear regression. The calculated rate constants were 2.03 $\mu m^2/hr$ (5.63×10^{-16} m^2/s) at 1600 °C, 4.76 $\mu m^2/hr$ (1.32×10^{-15} m^2/s) at 1700 °C, and 11.22 $\mu m^2/hr$ (3.12×10^{-15} m^2/s) at 1800 °C, respectively. A plot of the rate constant versus reciprocal temperature (Figure 10) allows for a determination of the activation energy for growth of the T_2 phase as 275.8 kJ/mol. A similar growth kinetics plot for the Mo_3Si phase is presented in Figure 11. In this case the calculated rate constants of Mo_3Si were 0.44 $\mu m^2/hr$ (1.21×10^{-16} m^2/s) at 1600 °C and 1.23 $\mu m^2/hr$ (3.41×10^{-16} m^2/s) at 1700 °C, which are slower than the growth rates of T_2. The Mo_3Si phase seems to continuously grow at 1600 and 1700 °C, but it exhibits a maximum in the layer thickness at 1800 °C. This indicates a possibility of either disappearance of the Mo_3Si phase after long term heat treatment or the operation of different growth kinetics behavior at 1800 °C. According to Bartlett et al [64Bar], the growth rate constant of Mo_3Si

Table 4. *Average effective interdiffusion coefficients for Si and B in the T_2 phase layer in the Mo_2B/Mo_5Si_3 diffusion couples annealed between 1600 and 1800 °C*

Temperature (°C)	Annealing time (hr)	$\tilde{D}_{Si}^{eff}$ (m^2s^{-1})	$\tilde{D}_{B}^{eff}$ (m^2s^{-1})
1600	805	9.40×10^{-16}	4.33×10^{-16}
1700	182	2.43×10^{-15}	1.50×10^{-16}
1800	100	8.17×10^{-15}	9.26×10^{-15}

produced in the $MoSi_2$-coated Mo system is 3.75×10^{-14} m^2/sec at 1600°C. The growth rates of T_2 and Mo_3Si produced in the Mo_2B/Mo_5Si_3 diffusion couples are about two orders of magnitude lower than that of Mo_3Si in the $MoSi_2$-coated Mo system, for thin Mo_3Si layer grew in the $MoSi_2$ coated Mo system and obeys the linear layer

growth kinetics. Therefore, long-term diffusion experiments are needed in order to provide a reliable analysis of the growth kinetics behavior.

Figure 5(b) and (c) show the BSE images of the cross-sections of diffusion couples annealed at 1600°C for 400 and 805 hours indicating a diffusion pathway of $Mo_2B/T_2/Mo_5Si_3$. The Mo_3Si phase has not been observed in these diffusion couples. The T_2 layer thickness measurements in the Mo_2B/Mo_5Si_3 diffusion couples annealed at temperatures (Figure 9) established that a diffusion control mechanism dominates the overall growth kinetics for the T_2 phase, which is influenced by the neighboring phases that change with time during heat treatment. In previous work, Dayananda *et al.* [99Day] proposed a method that determines the average interdiffusion coefficients from a single diffusion couple experiment. Due to limited homogeneity ranges of composition, the interdiffusion coefficients for Si and B in the T_2 phase could have approximately definite values. It should be noted that the interdiffusion coefficients with approximately consistent values over homogeneity ranges of composition could be expressed with the average effective interdiffusion coefficients, which is defined as the ratio of total interdiffusion flux over the diffusion zone to the corresponding concentration difference [96Day,99Tor]. The average effective interdiffusion coefficients for Si and B, $\tilde{D}_{Si}^{eff}$ and $\tilde{D}_{B}^{eff}$, obtained from concentration profiles of the Mo_2B/Mo_5Si_3 diffusion couples annealed between 1600 and 1800 °C are listed in Table 4, in which $\tilde{D}_{Si}^{eff} > \tilde{D}_{B}^{eff}$ at 1600 and 1700 °C and $\tilde{D}_{Si}^{eff} < \tilde{D}_{B}^{eff}$ at 1800 °C. Arrhenius plot of the average effective interdiffusion coefficients versus the reciprocal temperature informs that activation energies for Si and B diffusion are 348.01 and 492.28 kJ/mol (fig.12) that are larger than the activation energy for the T_2 phase layer growth. In this regard, the thermal energy can activate Si relatively easier than B at a temperature between 1600 and 1700 °C. At 1800 °C when the thermal energy is considered sufficiently enough in breaking bonds and overcoming the activation energy barrier, B atoms are likely to move faster than Si atoms because of the atomic size difference. It appears that below 1700 °C slower diffusing B limits growth of the T_2 phase layer and above 1800°C slower moving Si limits growth of the T_2 phase layer. This indicates that the diffusional growth kinetic behavior of the T_2 phase varies from the B-controlled kinetics at 1600 and 1700 °C to the Si-controlled kinetics at 1800 °C. In addition, the fact that the self-diffusion of Mo in pure Mo (bcc) is 1.5×10^{-17} m²/sec at 1600°C [79Mai] and the evaluated average effective interdiffusion coefficients are in the order of 10^{-16} m²/sec, is consistent with the sluggish growth rate of the T_2 phase. Therefore, interpretation of the kinetics data from these measurements is essential for understanding high temperature materials behavior.

2.5. Influence of Substitutional Alloying on Phase Stability

A common feature of the refractory metals is the high mutual solid solution solubility. This trend exists not only in the BCC solutions, but also extends to many intermediate phases (e.g. silicides, borides and aluminides). At the same time, the sensitivity of the T_2 phase stability to atomic size and off-stoichiometric site substitution suggests that refractory metal substitution for Mo can be an effective approach to controlling phase reactions.

This behavior has been examined by determining the effect of refractory metal substitution on the extent of the $Mo_{ss} + T_2$ two phase field and the influence of alloying on the solubility of metalloid constituents in T_2. Three

distinct types of behavior of metalloid solubility that can be discerned with refractory metal substitution. Alloying with Nb for instance tends to shift the metalloid solubility towards Si-rich values by lowering the B to Si ratio with increasing Nb levels. On the contrary, Cr substitution stabilizes the T_2 phase by altering the metalloid content toward the B-rich side resulting in a continuous increase of B to Si ratio in the T_2 phase with an increase in Cr substitution. Substitution with W or V on the other hand does not appear to cause a major shift in the B to Si ratio

It has been shown previously [84Fra] that most of the binary alloy T_2 (Me_5X_3) phases maintain an atomic radius ratio (r_{Me}/r_X) in a range of 1.2 to 1.5. This behavior leads to a size factor concept that is based upon a geometrical constraint to allow for optimum packing of the transition metal constituents with the metalloids. In ternary T_2 phases ($Me_5Xa_1Xb_2$) where the radius ratio is $r_{Me}/$ ($1/3 \, r_{Xa} + 2/3 \, r_{Xb}$), an increase in average metallic radius in the metal sites necessitates an expansion of the metalloid sites. This may be accomplished by enrichment of Si filling in the B lattice site at the trigonal prismatic hole, as exemplified in the case of Nb substitution. In fact, the relatively limited two-phase field of Mo(ss) + T_2 in the Mo-Si-B ternary system can also be enlarged by Nb substitution (Figure 1c) due to the continuous solution of both the (Mo,Nb) phase and the T_2 phase in the Mo-Nb-Si-B quaternary system as illustrated in Figure 13a. This is confirmed by a continuous shift in X-ray peak positions of the two phases after annealing at 1600°C for 200 hours (Figure 14a).

A continuous metallic solid solution which results in a reduction in the metallic atomic radius in the T_2 phase alters the solubility behavior of B and Si to accommodate the volume reduction in the metalloid sites. For example, there is a continuous increase of B solubility with a corresponding increase in Cr addition in the metal sites of the T_2 phase as illustrated in Figure 13b. In fact, Si atoms can be totally replaced forming the $(Cr,Mo)_5B_3$ phase. Similar to the Nb-Si-B system [95Vil], a large two-phase field is also present in the Cr-Mo-B system. Figure 14b shows the continuous shift in the X-ray peak positions indicating the reduction of the T_2 cell volume with increasing substitution level. It is worth noting also that there is a linear correlation between the corrected atomic size of the metal constituents and the cube root of the unit cell volume over a wide range of binary-based T_2 phases after including a necessary atomic size correction based on the Miedema electronegativity [84Fra]. This observation apparently can also be extended to the ternary-based Me_5SiB_2 phases where Me is a transition metal as shown in Figure 15a. Furthermore, it has been shown in binary-based T_2 phases that there is also a preferential dilation of the a parameter relative to the c parameter (Figure 15a) with the expansion of the crystal due to an increase in radius of the metal atoms. Figure 15b shows that a preferential dilation in the a parameter is consistently observed in the binary and ternary Me_5 (Si, B, Ge)$_3$ type T_2 phases including the Nb and Cr-substituted T_2 phases. Hence, the solubility behavior that can be judged in terms of the size factor concept provides a useful guidance in designing effective alloying strategies for the T_2 phase. Furthermore, the ability to predict the structural stability of the T_2 crystal with refractory metal substitution for Mo can be utilized to optimize the overall materials properties. In this context, the most critical issue in terms of taking the full advantage of the geometrical concept is to what extent the size factor can be implemented optimally for the phase stability analysis. The full extent of application to the geometrical rules has not been fully assessed. Hence, there is an immediate need not only to extend the experimental verification on the geometrical rules, but also to collaborate it with computer modeling. The impact of this assessment will affect not only the optimization of the multi-phase designs but only it will greatly influence the

development of the solidification microstructure. This is exemplified in the effect of refractory metal substitution on the solidification pathways and segregation in the Mo-rich Mo-Si-B alloys.

The large extent of solidification segregation in Mo-rich Mo-B-Si alloys is manifested by the presence of primary boride (Mo_2B and MoB) solidification products in alloys with compositions in the $Mo(ss)+T_2$ two-phase field. The Mo_2B primary solidification precludes the attainment of eutectic $Mo(ss) + T_2$ alloy microstructures as shown in Figure 16 which presents the liquidus projection [00Nun] and as illustrated by the as-cast structure of Mo-7Si-14B in Figure 17a. To avoid the Mo_2B primary phase, the liquidus projection suggests that at least the formation of the four-phase equilibria of Class II reaction ($Mo_2B + L => Mo(ss) + T_2$) must be avoided. Since the equilibrium point is outside the two-phase field, the compositions used will always be within the three-phase field of $Mo(ss) + T_2 + Mo_3Si$. This may present some difficulties particularly since the preceding reaction of Class I ($L => Mo(ss) + T_2 + Mo_3Si$) may be bypassed by a slight undercooling due to the relatively shallow liquidus surfaces for Mo_3Si and T_2 and, as a consequence, the monovariant eutectic structure of $Mo_3Si + T_2$ forms instead. The presence of a relatively brittle $MoSi_3$ constituent may not be desirable. It is therefore necessary to alter the primary Mo_2B solidification event.

One strategy to produce the $Mo(ss) + T_2$ two-phase microstructure directly from the melt is to suppress the primary boride phases [99Sak-b] . Rapid Solidification Processing (RSP) can yield a fine two-phase microstructure by bypassing the formation of the boride phase. The solidification path of the undercooled melt is simplified into either $Mo(ss)$ or T_2 primary solidification followed by the $Mo(ss) + T_2$ eutectic formation. Due to the very short diffusion distances in this fine microstructure, subsequent annealing at a relatively low temperature such 1200°C for 150 hours is sufficient to yield a uniform sub-micron two-phase $Mo(ss) + T_2$ microstructure [99Sak-b].

Another effective design strategy for altering the solidification pathway is to apply selected quaternary additions. In fact, the systematic substitution of Mo by Nb has been shown to reduce the extent of Mo_2B primary formation (Figure 17b). The reduction in the Mo_2B liquidus extension may be due to the fact that the amount of Nb substitution for Mo in Mo_2B is limited [71Kuz]. On the other hand, a large degree of Nb substitution for Mo in both the bcc $Mo(ss)$ phase as well in the T_2 phase has been established (Figure 13a). As a result, two-phase [Mo,Nb] (ss) + T_2 microstructures can be produced directly from the melt as shown in Figure 17c.

In alloys where the nominal composition is no longer in the $Mo(ss) + T_2$ two-phase field, but rather in the three-phase field of $Mo(ss) + T_2 + Mo_3Si$, refractory metal (RM) substitution also may also affect the solidification pathways significantly. The substitution can modify the final solidification reactions that involve the Mo_3Si-rich eutectic. As for the case of the Mo_2B phase, the liquidus surface extension for the Mo_3Si phase into the quaternary system with refractory metal substitutions such as Nb or W, has been found to be quite limited. This is due to the limited solubility of Nb or W in the Mo_3Si phase [65Sav]. In contrast, the T_2 as well as the T_1 phase forms a continuous solid solution with Nb and W substitution and hence, a three phase field of $(Mo,RM) + T_2 + T_1$ can be stabilized in the quaternary system of Mo-Nb-Si-B as well as in Mo-W-Si-B. Accordingly, the modifications in the phase equilibria with increasing refractory metal substitution are reflected by the formation of a three-phase eutectic of $(Mo,RM) + T_2 + T_1$ as exemplified in Figure 17c. With increasing substitution of Mo by Nb or W, the Mo-Si-B based three-phase eutectic of $(Mo,RM)_3Si + T_2 + (Mo,RM)$ terminates and the solidification pathway proceeds with

the formation of five-phase equilibria of : $L + (Mo,RM)_3Si => (Mo,RM) + T_2 + T_1$. A significant consequence of this reaction and the new phase equilibrium is the synthesis of a microstructure with a uniform dispersion of (Mo,RM) ductile phase with compatible high melting T_2 and T_1 phases [65Sav]. The new multi-phase configuration stabilized by these refractory metals may be optimized to take advantage of the benefits of high oxidation and creep resistance of T_1 and T_2 phases and the toughness and ductility of the bcc phase.

It is important to point our here that while the new solidification pathways based on the establishment of the new phase equilibrium offers an attractive opportunity for multi-phase microstructure design based upon the three phase interwoven morphology shown in Figure 17c, there are at least two critical issues that have not been fully elucidated;

(1) The resolution on the solidification pathway(s) leading to the new eutectic structure,

(2) The overall impact of the refractory alloying being added to stabilize the new phase equilibrium, particularly as it pertains to the mechanical properties.

The current analysis on the solidification pathways resulting the three-phase $(Mo,RM) + T_2 + T_1$ eutectic suggests that there must be an intermediate stage that involves formation of three separate two-phase eutectic structures of $(Mo,RM) + T_2$, $(Mo,RM + T_1$ and $T_2 + T_1$ that precedes the formation of the $(Mo,RM) + T_2 + T_1$ three-phase eutectic. While both $(Mo,RM) + T_2$ and $T_2 + T_1$ eutectic structures have been observed in the Mo-Si-B system, the $(Mo,RM) + T_1$ eutectic structure as not. The eutectic $(Mo,RM) + T_1$ eutectic apparently develops instead from the Mo-RM-Si ternary systems such as Mo-Nb-Si and Mo-W-Si. Figure 18a shows the TEM image of the $(Mo,Nb) + T_1$ eutectic structure. Similar to our previous finding in the $Mo(ss) + T_2$, the eutectic structure [00Nun], the two-phase $(Mo,Nb) + T_1$ eutectic structure also develops unique crystallographic relations as depicted in Figure 18b. A similar existence of $BCC + T_1$ eutectic structure is also expected in the Mo-W-Si system. It is important to point out that the two ternary systems (Mo-W-Si and Mo-Nb-Si) share one unique characteristic; both allow a very limited refractory substitution in the Mo_3Si phase. The importance consequence of the limited stability of the Mo_3Si phase is the formation a large two-phase field of the $(Mo,RM) + T_1$ which leads to the stabilization of the $(Mo,Nb) + T_1$ eutectic structure through the Class II invariant reaction of $(Mo,RM)_3Si + L => (Mo,RM) + T_1$. While the invariant reaction in the RM-Si-B system appears to readily facilitate the three-phase eutectic solidification reaction, the two invariant points in the Mo-Si-B require more intermediate solidification stages. The two invariant points correspond to solidification reactions of the Class I type reaction $L => Mo + T_2 + Mo_3Si$ and the Class II type reaction of $T_1 + L => T_2 + Mo_3Si$. Neither one of these reactions will directly lead to a five –phase solidification reaction of $L + (Mo,RM)_3Si => (Mo,RM) + T_2 + T_1$ as suggested above. Therefore, modifications by the RM substitution on the invariant points must take place. For example, the Class I reaction of $L => Mo + T_2 + Mo_3Si$ must be altered to 'favor' four-phase solidification reaction of $(Mo,RM)_3Si + L => (Mo,RM) + T_2$. Clearly, further refinement in the detailed sequences in the solidification pathways is critical and requires a more detailed examination.

It is well recognized that for a given amount of RM substitution level, the solubility of the alloying element in the BCC, T_2 and T_1 in most cases is not necessarily the same. Therefore, it is necessary, especially for the multi-phase designs, that the impact on the materials properties not only on the overall bulk materials, but also on the

individual phases be fully evaluated. For this purpose, nano-indentation techniques play a significant role in discerning the mechanical properties of each phase in the microstructure. In the current work, with our collaboration with Prof. M Goeken from University of Saarbrücken, the microstructural mechanical properties of the ternary Mo-Si-B alloys which consisted of three phases; Mo(ss) , T_2 phases have been successfully evaluated [01Goe] . As shown in Table 5, the nano-indentation technique allows us to identify the differences in both the hardness and the elastic modulus of each phases in the microstructure. Furthermore, the occurrence of 'pop-in' phenomenon which corresponds to the activation of yielding and plasticity in the T_2 phase at ambient temperature has been identified as shown in Figure 19 [01Goe]. It is expected that a similar technique will be implemented into the analysis on the mechanical properties of the three-phase (Mo,RM) + T_2 + T_1 microstructures.

Table 5 Microstructural mechanical properties of Mo-10Si-20B (at. %) Alloys
(Heat treatment was1600°C for 150 hours and the nanoindentation test was conducted using Berkovich tip (XP-DCM) with 1 mN maximum load)

Mechanical Properties	Mo(ss) Phase		T_2 Phase	
	As-Cast	Heat-Treated	As-Cast	Heat-Treated
Elastic Modulus (GPa)	301	321	259	320
Hardness (GPa)	13	8.5	19.0	22.2

2.6. Analysis on the Solidification Reactions in Mo-RM-Si-B Alloys

The key in understanding the formation of the new three-phase BCC + T_2 + T_1 eutectic structure (Figure 20a) in the quaternary Mo-RM-Si-B system has been the identification of the preceding reactions leading to the invariant reaction that yield the three-phase eutectic [01Per]. Analysis on the solidification pathways shows that the three-phase eutectic is produced from the five-phase solidification reaction (figure 20b):

$$(Mo,RM)_3Si + L \Rightarrow BCC + T_2 + T_1$$
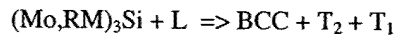
Typically, there is a strong preferential solute partitioning during the growth of the three-phase eutectic as illustrated in figure 20c. This may be useful for further alloying strategies when there is a need to control different levels of alloying addition in each phase. The formation of an invariant point is preceded by the formation of three Class II solidification reactions that generate three types of two-phase eutectics:

$$(Mo,RM)_3Si + L \Leftrightarrow BCC + T_2$$
$$(Mo,RM)_3Si + L \Leftrightarrow T_2 + T_1$$
$$(Mo,RM)_3Si + L \Leftrightarrow BCC + T_1$$
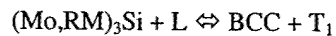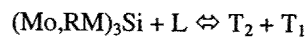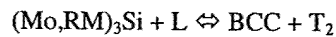
The first two types of eutectic structures (BCC+ T_2 and T_2 + T_1) have been previously observed in the Mo-Si-B system. The third one, the two-phase eutectic of BCC + T_1 phases, on the other hand, can only be possible through refractory metal substitution for Mo. In this case, both Nb and W substitutional alloying can be used to produce the third two-phase eutectic. In each alloying case, the extension of substitutional alloying for the Mo_3Si phase is much more limited that the T_1 or BCC phase. In fact, in both phases, there is a continuous (Mo,RM) solid solution. TEM analysis of the crystallographic orientation suggests the following relationship (Figure 18):

$$[001]T_1//[110]BCC, (1,-1,2)T_1//(550)BCC$$
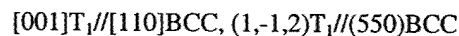
One of the advantages of the three-phase eutectic is the fact that BCC phase can be distributed in the cast alloys up to the last stage of the solidification reactions. For example, with alloys that solidifies with BCC as the primary phase, the reactions may proceed as follows:

```
                        ┌──────────────────┐
                        │   BCC Primary    │
                        └──────────────────┘
          ┌─────────────────────┼─────────────────────┐
          ▼                      ▼                      ▼
┌──────────────────┐  ┌──────────────────┐  ┌──────────────────┐
│ BCC + T2 Eutectic│  │ BCC + T1 Eutectic│  │     T2 + T1      │
└──────────────────┘  └──────────────────┘  └──────────────────┘
          │                      ▼                      │
          └───────────►┌──────────────────────┐◄────────┘
                       │ BCC + T₂ + T₁ Eutectic│
                       └──────────────────────┘
```
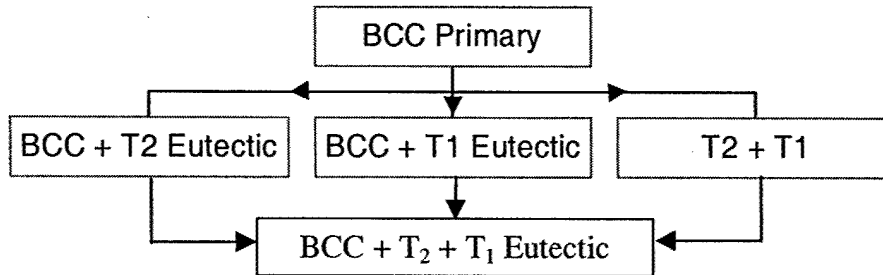
In this case, the distribution of the BCC phase can be optimized so as to improve the fracture toughness of the overall microstructures.

The choice of the primary phases as well as solidification pathways to proceed will depend on the materials property requirements. For example, if improved elevated temperature strength is required, the use of T_2 or T_1 primary phases may be preferable. Similarly, one may also consider the use of co-primary of T_2 or T_1 phase. For example, Figure 21 shows an example of microstructures from cast-alloys that solidifies with $T_1 + T_2$ as the co-primary phases. The two primary phases are surrounded by the three-phase eutectic consisting of BCC + T_2 + T_1 phases.

3. Summary of Research Highlights

From a foundation of the established phase equilibrium in the Mo-Si-B system at 1600°C a systematic examination has been initiated into the phase stability and solidification pathways that constitute essential factors in developing a control of the microstructural evolution. The ternary T_2 (Mo_5SiB_2) phase is clearly a key member of any alloy design since it develops equilibria with each of the binary boride and silicide phases for Mo-rich alloys in the Mo-Si-B system. The T_2 phase is not a stoichiometric compound, but shows a compositional existence range that extends mainly to B-rich and Si-rich departures from stoichiometry. Unlike most of the metal silicides, the T_2 phase also exhibits temperature dependent solubility for Mo which is manifested by the Mo(ss) precipitation reaction upon annealing. These observations represent a clear indication that constitutional defects are critical to understanding the stability of the T_2 phase. During reactive diffusion between Mo_2B and Mo_5Si_3, the T_2 phase is synthesized. Analysis of the growth kinetics yields diffusivities of about 10^{-16} m^2/s at 1600°C in the T_2 phase. Following conventional solidification processing Mo-Si-B alloys exhibit extensive segregation in the form of non-equilibrium phases. For example, the stoichiometric T_2 alloy composition follows a complex solidification path involving: $L \rightarrow MoB + L_1$ $\rightarrow MoB + T_2 + L_2 \rightarrow MoB + T_2 + Mo_5Si_3 + L_3 \rightarrow MoB + T_2 + Mo_5Si_3 + Mo_{ss} + L_4 \rightarrow MoB + T_2 + Mo_5Si_3 + Mo_{ss} + Mo_3Si$. The homogenization of the as-cast structure to establish the equilibrium phase constitution is difficult during solid state annealing due to sluggish diffusion kinetics. Alternate processing by rapid solidification or selected alloying such as partial substitution of Mo by Nb or W has been demonstrated to effectively reduce segregation to yield two phase ($Mo_{ss}+T_2$) and a new three-phase ($RM+T_1+T_2$) microstructures directly during solidification. At the

same time, the observed modification of the relative phase stability due to alloying reveals the central role that the atomic sizes and the possible constitutional defect structure play in the structural stability of the T_2 phase. The current understanding provides effective guidance to identify the key experimental measurements in order to formulate a computational thermodynamic model that can leverage the known behavior to optimize new multiphase designs and processing.

4. Publication List

During a research program, substantial time intervals often elapse between the completion of a research study, submission of a manuscript and the final appearance of a paper in print. As a result, the following list gives publications in preparation as well as those in print of in press. (The papers noted by an asterisk are invited).

1) R. Sakidja, G. Wilde, H. Sieber and J. H. Perepezko, in *High-Temperature Ordered Intermetallic Alloys VIII* (edited by E. P. George, M. Yamaguchi, M. J. Mills), *Mater. Res. Soc. Proc. 552*, Pittsburgh, PA, pp. KK6.3.1 (1999).

2) R. Sakidja, H. Sieber and J. H. Perepezko, *Philosophical Magazine Letters*, **79** [6], pp. 351-357 (1999).

3) C. A. Nunes, R. Sakidja, Z. Dong, and J. H. Perepezko, "Liquidus Projection for the Mo-rich portion of the Mo-Si-B ternary system, Intermetallics, 8[4] pp. 327-37 (2000).

*4) R. Sakidja, J. Myers, S. Kim and J. H. Perepezko, the International Journal of Refractory Metals and Hard Materials, 18[4-5], 193 (2000).

5) G. Wilde, R. Sakidja, Z. Dong and J. H. Perepezko, "Microstructural development and phase stability of Mo_{ss}-Mo_5SiB_2 in-situ composites", *High Temperature Materials Chemistry* (ed. K. Hilpert, F. W. Froben, L. Singheiser, S. F. Jülich and R. Energietechrik), 15, pp. 157-160 (2000).

6) J. H. Fournelle, J. J. Donovan, S. Kim and J. H. Perepezko, "Analysis of Boron by EPMA: correction for dual Mo and Si interferences for phases in the Mo-B-Si system", *Proceeding of 2nd Conference of International Union of Microbeam Analysis Societies (IUMAS)*, pp.425-426, 2000.

7) S. Kim, R. Sakidja, Z. Dong, J. H. Perepezko and Y. W. Kim, "Growth of the Mo_5SiB_2 Phase in a Mo_5Si_3/Mo_2B Diffusion Couple", in *High Temperature Ordered Intermetallic Alloys IX* (ed. J. H. Schneibel, S. Hanada, K. J. Hemker, R. D. Noebe and G. Sauthoff) *Mater. Res. Soc. Symp. Proc. 646*, Pittsburgh, PA, pp. N5.42.1-N5.42.6 (2001).

*8) J. H. Perepezko, R. Sakidja and S. Kim, "Phase Stability in Processing and Microstructure Control in High Temperature Mo-Si-B Alloys", in *High Temperature Ordered Intermetallic Alloys IX* (ed. J. H. Schneibel, S. Hanada, K. J. Hemker, R. D. Noebe and G. Sauthoff) *Mater. Res. Soc. Symp. Proc. 646*, Pittsburgh, PA, pp. N4.5.1-N4.5.12 (2001).

9) J. H. Perepezko, R. Sakidja, S. Kim, Z. Dong and J. S. Park, "Multiphase microstructures and stability in high temperature Mo-Si-B alloys", in *Structural Intermetallics 2001* (ed. K. J. Hemker, D. M. Dimiduk, H. Clemens, R. Darolia, H. Inui, J. M. Larsen, V. K. Sikka, M. Thomas and J. D. Whittenberger), TMS, Warrendale, PA, pp. 505-514 (2001).

10) M. Göeken, R. Sakidja, W. D. Nix and J. H. Perepezko, "Microstructural Mechanical Properties and Yield Point Effects in Mo Alloys", *Materials Science and Engineering A*, 319-321, pp. 902-908 (2001).

11) "Transition Metal Substitutional Alloying and Phase Stability in the Mo-Si-B System", R. Sakidja, S. Kim, J.S. Park and J.H. Perepezko, MRS Symposium Proc.(in press)

12) R. Sakidja, S. Kim and J. H. Perepezko, "Multi-phase stability design in high-temperature BCC + T_2 + T_1 three-phase alloys," in preparation (2002).

13) R. Sakidja and J. H. Perepezko," On the mechanism of polymorphic phase transition in Nb-rich T_2 Phase," in preparation (2002).

Presentations

1-7) The publications (4-9,11) were published in the proceedings of the respective conferences and involved presentations as well.

*8) J. H. Perepezko, R. Sakidja, J. Myers and S. Kim, "Microstructural Designs in High-Temperature (Mo,Nb)-Si-B Alloys, " presented at the *TMS 1999 Annual Meeting* in San Diego, CA, (Feb 28-Mar 4, 1999)

9) R. Sakidja and J. H. Perepezko, " The effect of refractory metal substitution on the stability of Mo(ss) + T_2 two-phase field in the Mo-B-Si system", presented in the Poster Session at *the Gordon Conference on Physical Metallurgy*, held at Plymouth, NH, July 23-28, 2000.

10) J. H. Perepezko, " Phase Stability and Microstructural Control in High Temperature (Mo,Nb)-Si-B Alloys," presented in AFOSR Contractor Workshop held at St. Louis, MO, October 12-13,2000.

11) J. H. Perepezko, "Multiphase Microstructures and Phase Stability in High Temperature (Mo,RM)-Si-B Alloys," presented in AFOSR Joint Annual Review of Metallic & Ceramic Materials Program held at Snowbird, UT, August 19-21, 2001.

12) J. H. Perepezko, "Multiphase Microstructures and Phase Stability in High Temperature (Mo,RM)-Si-B Alloys," presented in AFOSR Joint Annual Review of Metallic & Ceramic Materials Program held at Bar Harbor, ME, August 2002.

7. REFERENCES

[01Goe] Goeken, M., *et al.*, Materials Science and Engineering A, 2001. **319-321**: p. 902-908.

[01Kim] Kim, S., *et al.*, in *High Temperature Ordered Intermetallic Alloys IX*, J.H. Schneibel, *et al.*, Editors. 2001, MRS: Pittsburg, PA. p. N5.42.1.

[01Raw] Rawn, C.J., *et al.*, Intermetallics, 2001. **9**: p. 209.

[00Alf] Alfe, D., *et al.*, Int. J. Quantum Chem., 2000. **77**: p. 871.

[00Fou] Fournelle, J.H., *et al.* . in *Proceeding of 2nd Conference of International Union of Microbeam Analysis Societies (IUMAS)*. 2000. Kailua-Kona, Hawaii, July 9-13.

[00Fu] Fu, C.L. and X. Wang, Phil. Mag. Lett., 2000. **80**: p. 683.

18

[00Hue] Huebsch, J.J., *et al.*, Intermetallics, 2000. **8**: p. 143.

[00Nun] Nunes, C.A., *et al.*, Intermetallics, 2000. **8**: p. 327.

[00Ros] Rosales, I. and J.H. Schneibel, Intermetallics, 2000. **8**: p. 885.

[00Sak] Sakidja, R., *et al.*, The International Journal of Refractory Metals and Hard Materials, 2000. **18**(4-5): p. 193.

[99Day] Dayananda, M.A. and Y.H. Sohn, Metall. Mater. Trans. A, 1999. **30A**: p. 535.

[99Sak-a] Sakidja, R., H. Sieber, and J.H. Perepezko, Phil. Mag. Lett., 1999. **79**: p. 351.

[99Sak-b] Sakidja, R., *et al.*, in *High Temperature Ordered Intermetallic Alloys VIII*, E.P. George, M. Yamaguchi, and M.J. Mills, Editors. 1999, MRS: Pittsburgh, PA. p. KK6.3.1.

[99Sch] Schneibel, J.H., *et al.*, Mater. Sci. and Eng. A, 1999. **1-2**: p. 78.

[99Tor] P.C. Tortorici and M.A. Dayananda, Mater. Sci. and Eng. A, A261, 64, 1999

[98Sak] Sakidja, R., H. Sieber, and J.H. Perepezko, in *Molybdenum and Molybdenum Alloys*, A. Crowson, *et al.*, Editors. 1998, TMS: Warrendale, PA. p. 99.

[98Sch] Schneibel, J.H., *et al.*, Scripta Mater., 1998. **38**: p. 1169.

[97Nun] Nunes, C.A., R. Sakidja, and J.H. Perepezko, in *Structural Intermetallics 1997*, M.V. Nathal, *et al.*, Editors. 1997, TMS: Warrendale, PA. p. 831.

[97Per] Perepezko, J.H., *et al.*, in *High Temperature Ordered Intermetallic Alloys VII*, C.C. Koch, *et al.*, Editors. 1997, MRS: Pittsburgh, PA. p. 1.

[96Day] M.A. Dayananda, Mater. Trans. A, 27A, 2504, 1996

[95And] Anderson, I.M., A.J. Duncan, and J. Bentley, Mater. Res. Soc. Symp. Proc., 1995. **364**: p. 443.

[95Gas] Gaskell, D.R., *Introduction to the Thermodynamics of Materials*. 1995, Washington, DC: Taylor & Francis.

[95Vil] Villars, P., A. Prince, and H. Okamoto, in *Handbook of Ternary Alloy Phase Diagrams*. 1995, ASM International: Materials Park, Ohio. p. 5520.

[93Tho] Thom, A.J., *et al.*, in *Processing and Fabrication of Advanced Material for High Temperature Applications III*, T.S. Srivitsan and V.A. Ravi, Editors. 1993, TMS: Warrendale, PA. p. 413.

[92Boe] Boettinger, W.J., J.H. Perepezko, and P.S. Frankwitcz, Mater. Sci. and Eng., 1992. **A155**: p. 33.

[92Dim] Dimiduk, D.M., D.B. Miracle, and C.H. Ward, Mater. Sci. and Tech., 1992. **8**: p. 367.

[92Kub] Kubaschewski, O., C.B. Alcock, and P.J. Spencer, *Materials Thermochemistry*. 1992, Oxford, UK: Pergamon Press.

[92Sha] Shah, D.M., *et al.*, Mater. Sci. and Eng., 1992. **A155**: p. 45.

[92Vas] Vasudevan, A.K. and J.J. Petrovic, Mater. Sci. and Eng., 1992. **A155**: p. 1.

[91Kim] Kim, Y.W. and D.M. Dimiduk, JOM, 1991. **43**: p. 40.

[90Dys] Dyson, B.F. and M.M. Lean, JISI Int., 1990. **30**: p. 802.

[87Kir] Kirkaldy, J.S. and D.J. Young, *Diffusion in the Condensed State*. 1987, London, UK: Institute of Metals.

[87Ros] Ross, E.R. and C.T. Sims, in *Superalloys II*, C.T. Sims, Editor. 1987, John Wiley & Sons, Inc.: New York, NY. p. 97.

[87Sto] Stoloff, N.A., in *Superalloys II*, C.T. Sims, Editor. 1987, John Wiley & Sons, Inc.: New York, NY. p. 61.

[85Atk] Atkinson, K., *Elementary Numerical Analysis*. 1985, New York, NY: John Wiley & Sons.

[84Fra] Franceschi, E.A. and F. Ricaldone, Revue de Chimie Minerale, 1984. **21**: p. 202.

[83Bir] Birks, N. and G.H. Meier, in *Introduction to High Temperature Oxidation of Metals*. 1983, E. Arnolds Ltd.: London, UK. p. 54.

[79Mai] Maier, K., H. Mehrer, and G. Rein, Z. Metallkde., 1979. **90**: p. 271.

[71Kuz] Kuz'ma, Y.B., Soviet Powder Metallurgy and Metal Ceramics, 1971. **10**: p. 298.

[65Sav] Savitskiy, E.M., *et al.*, Russian Metall., 1965. **2**: p. 91.

[64Bar] Bartlett, R.W., P.R. Gage, and P.A. Larssen, Trans. AIME, 1964. **230**: p. 1528.

[58Aro] Aronsson, B., Acta Chemica Scandinavica, 1958. **12**: p. 31.

[57Now] Nowotny, H., E. Dimakopoulou, and H. Kudielka, Mh. Hem., 1957. **88**: p. 180.

a)

b)

c)
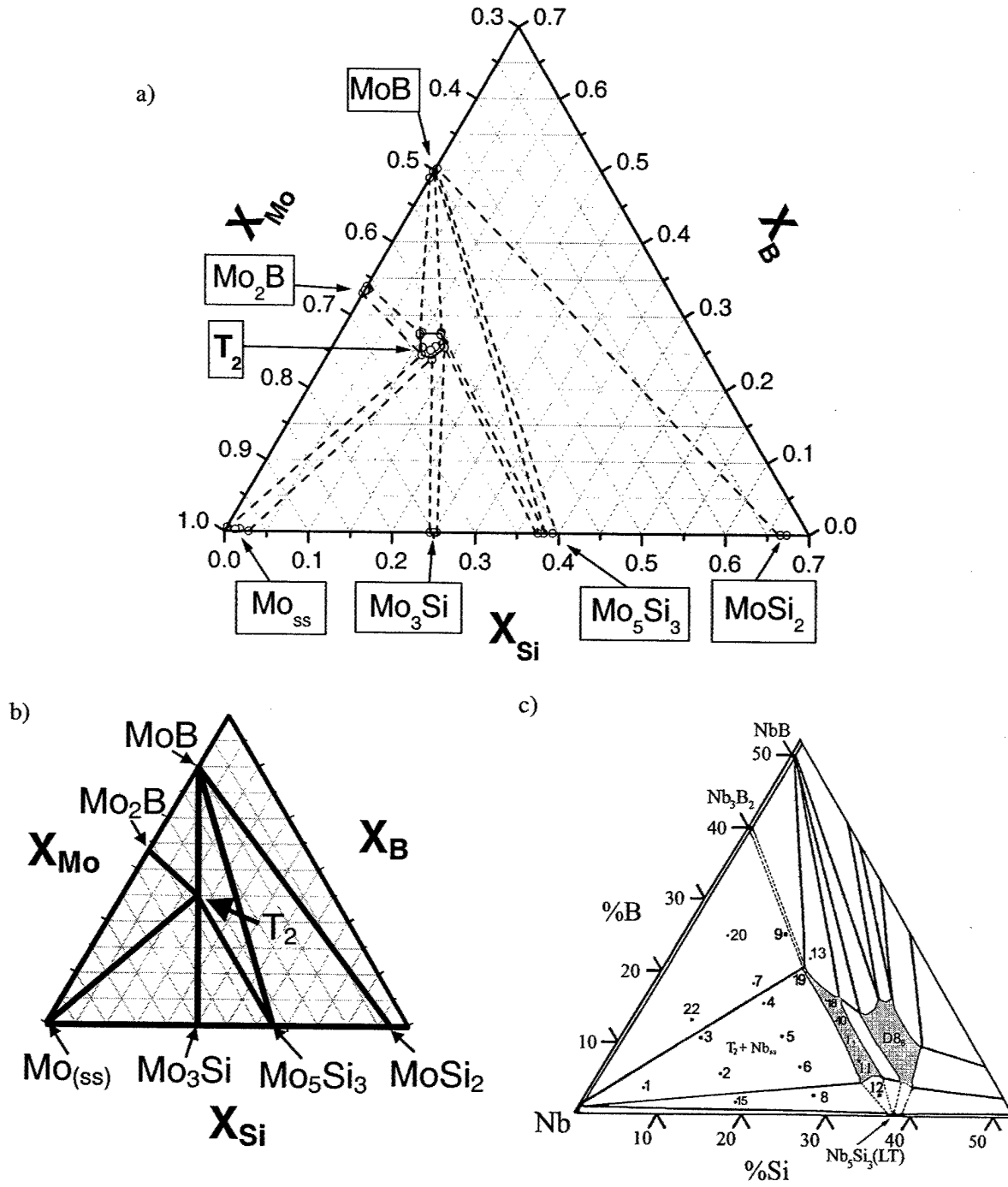
Figure 1 a) Isothermal section in the Mo-rich portion of Mo-Si-B system at 1600 °C, b) Calculated isothermal section c) The ternary isothermal section of the metal-rich ternary system of Nb-Si-B at 1600°C
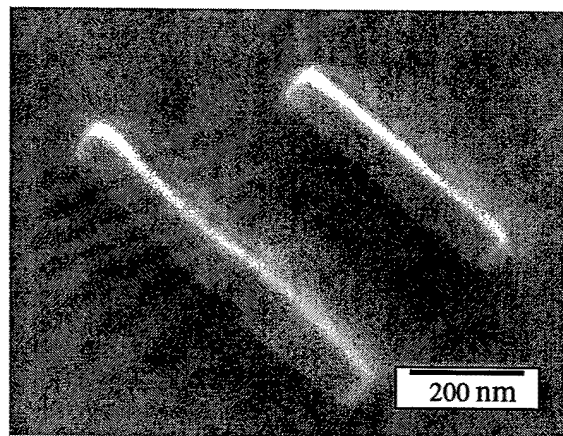
Figure 2 Mo(ss) precipitates in the T_2 phase matrix
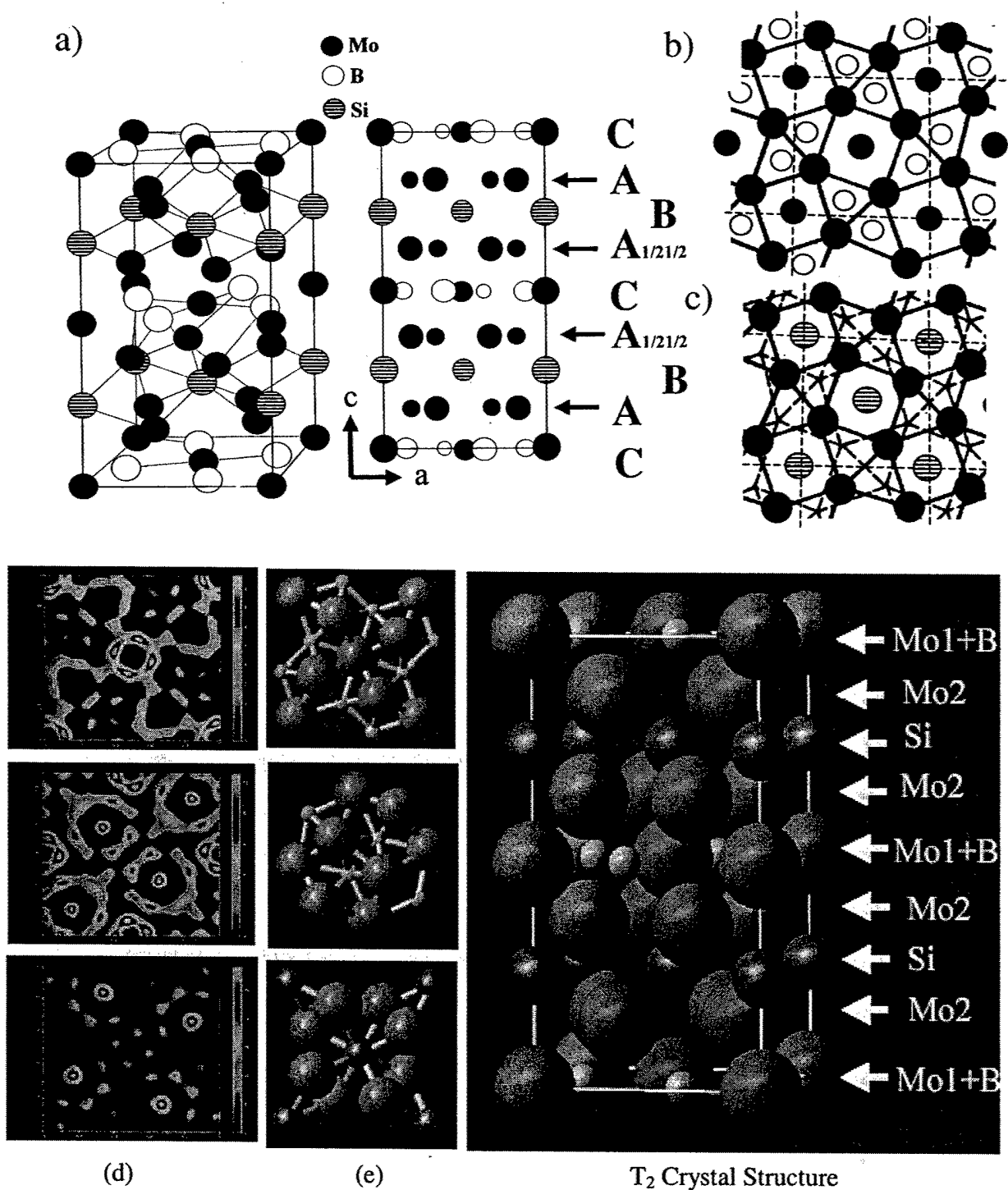
Figure 3 a) Crystal structure of T_2 phase (space group I4/mcm, D8$_1$) showing the layer stacking arrangements with projections along c axis for b) A-A stacking and c) A-A$_{1/21/2}$ stacking. (d) A series of selected slices of Slant-plane Fourier map along the c axis derived from the x-ray refinement of single crystal T_2. The intensities reflect the total electron density and reveal the presence of multi-directional bonding in the T2 phase as illustrated in (e).
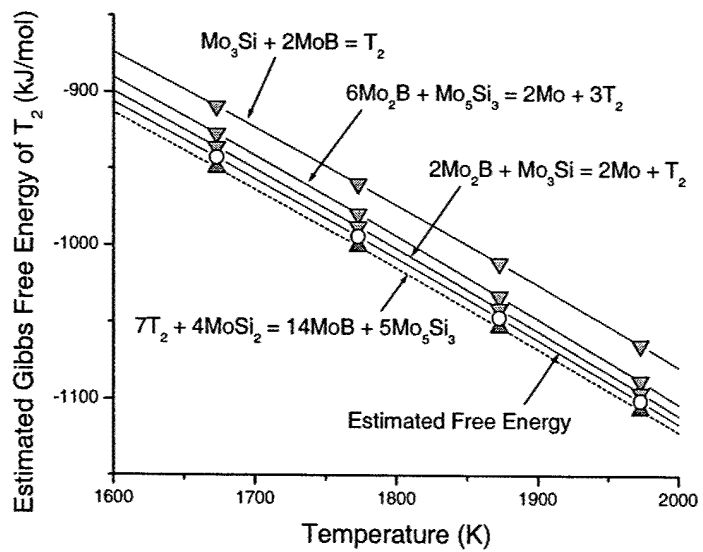
Figure 4 Estimation of the Gibbs free energy of the T_2 phase
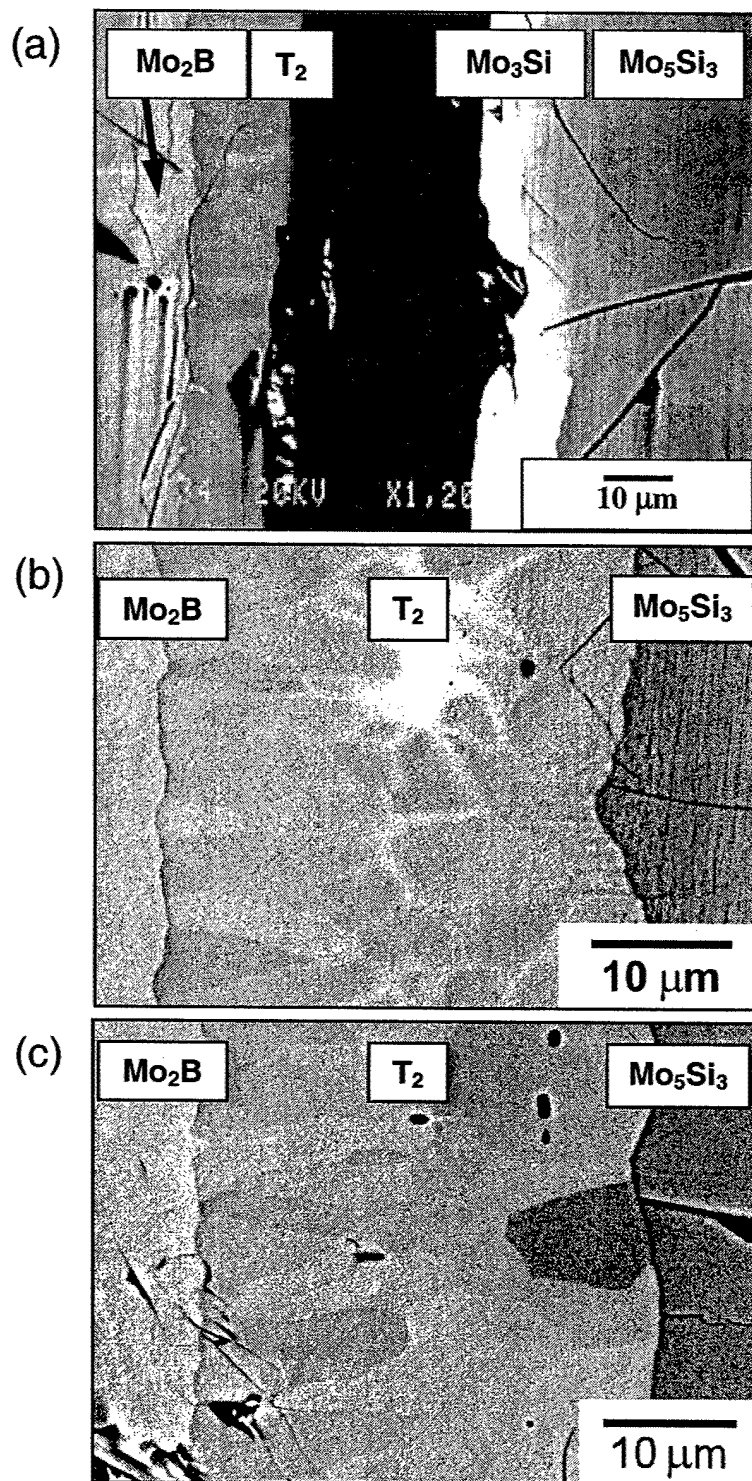
Figure 5 BSE images of cross-sections of the Mo_2B/Mo_5Si_3 diffusion couples heat-treated at 1600°C for (a) 100, (b) 400 and (c) 805 hrs
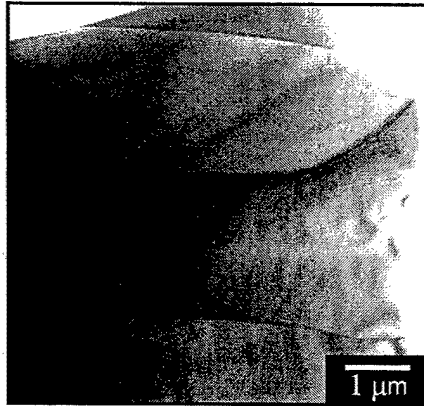
Figure 6   TEM image of the T_2 phase revealing a columnar growth
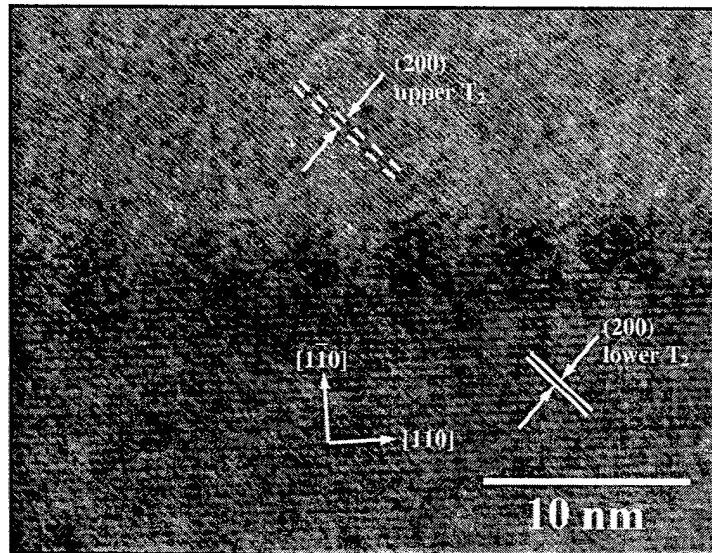
Figure 7 High Resolution TEM image of the T_2 grain boundary showing a low angle boundary
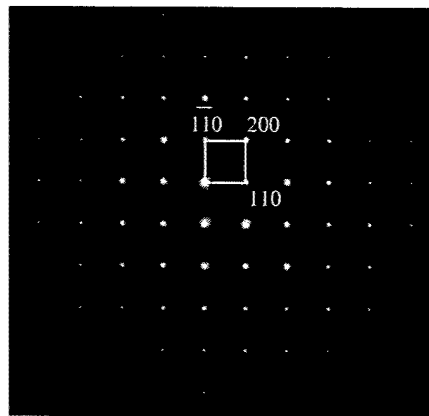
Figure 8 Electron diffraction pattern on the T_2 phase (001)
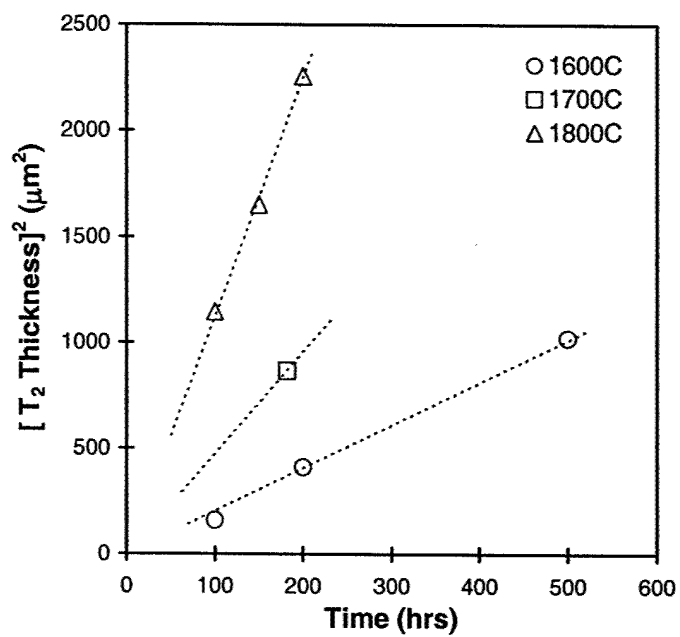
Figure 9 Plot of [thickness]^2 for the T_2 phase versus annealing time. Fit is based upon negligible initial thickness for the T_2 phase
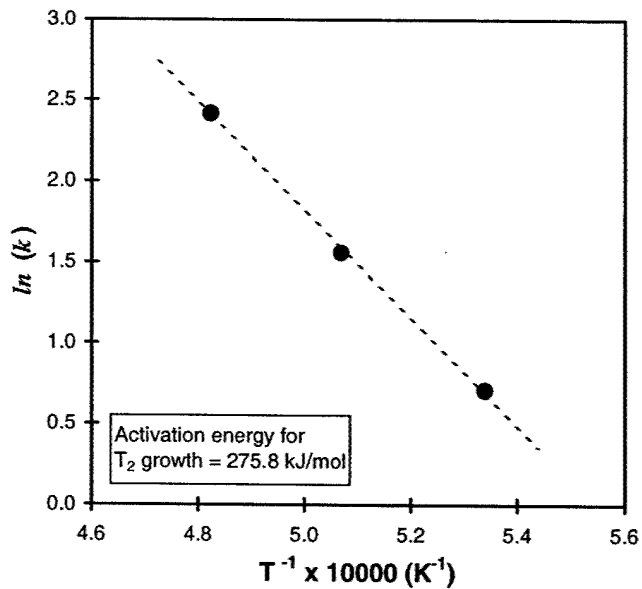
Figure 10 Plot of the rate constant of the T_2 phase versus reciprocal temperature
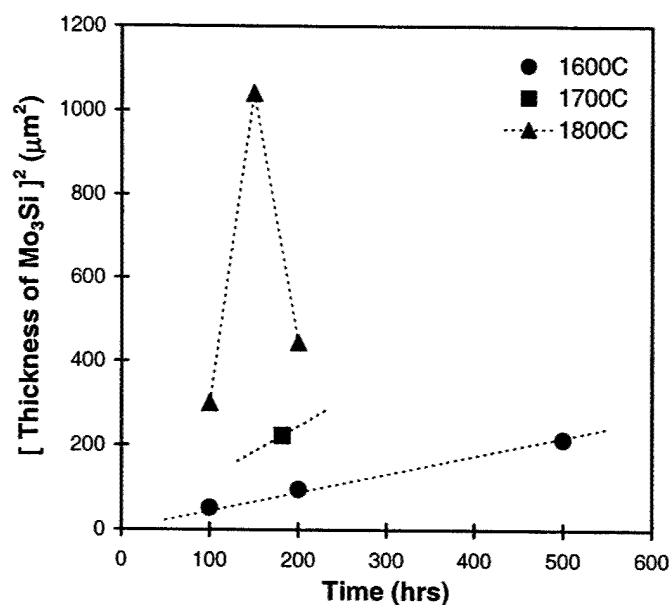
Figure 11 Plot of [thickness]^2 for the Mo$_3$Si phase versus annealing time
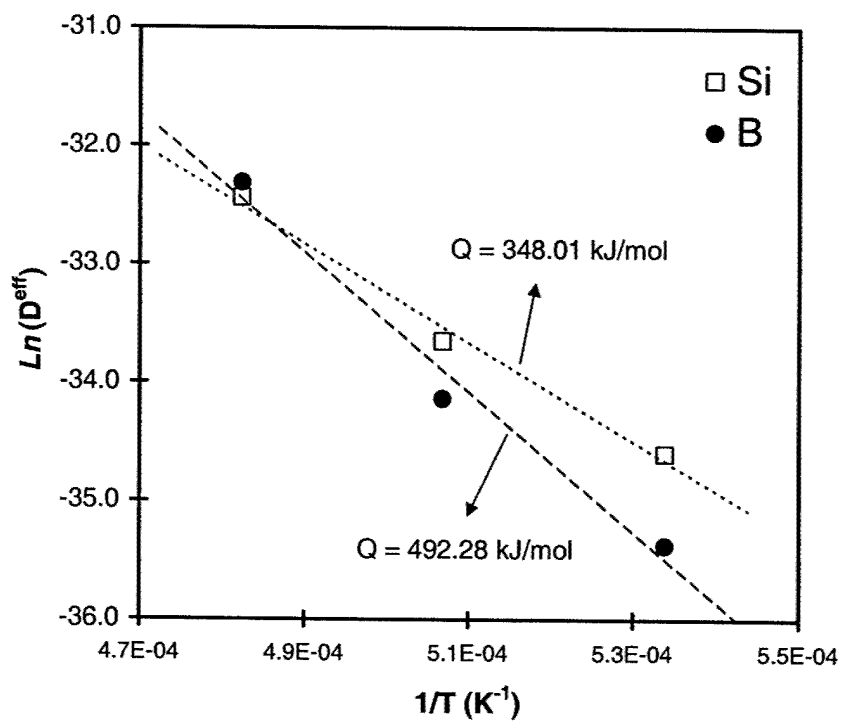
Figure 12 Arrhenius plot of the average effective interdiffusion coefficients versus the reciprocal temperature, which is showing that the activation energies for Si and B diffusion in the T$_2$ phase are 348.01 and 492.28 kJ/mol, respectively
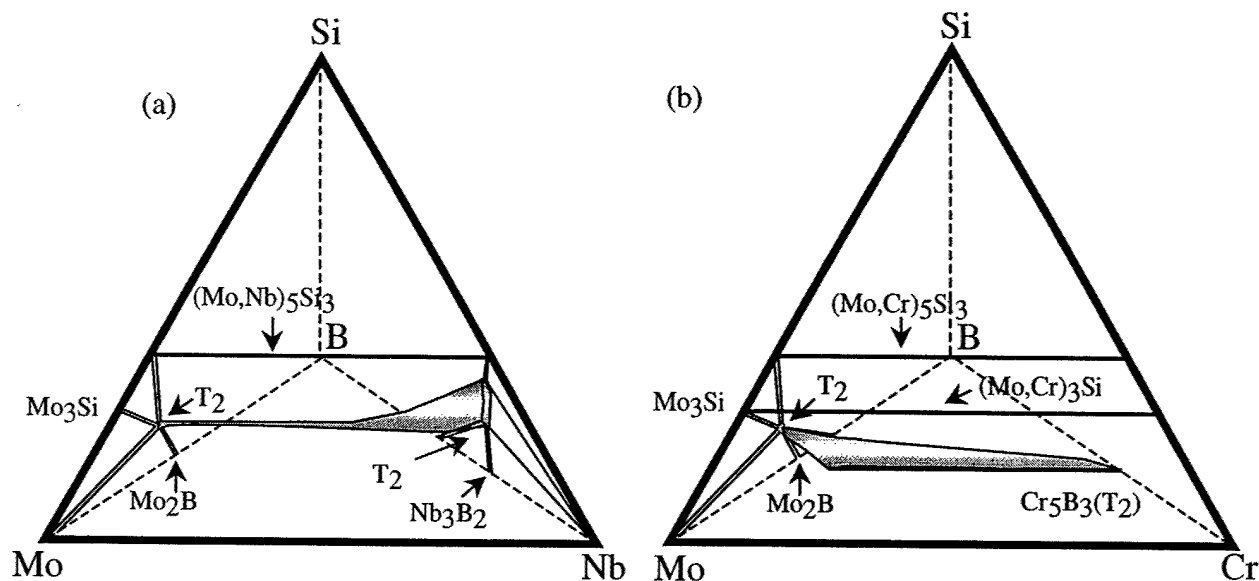
Figure 13 Illustrative diagrams showing the extension of the T_2 phase field in the a) Mo-Nb-Si-B and b) Mo-Cr-Si-B quaternary systems. To aid in visualization only relevant phases are indicated.
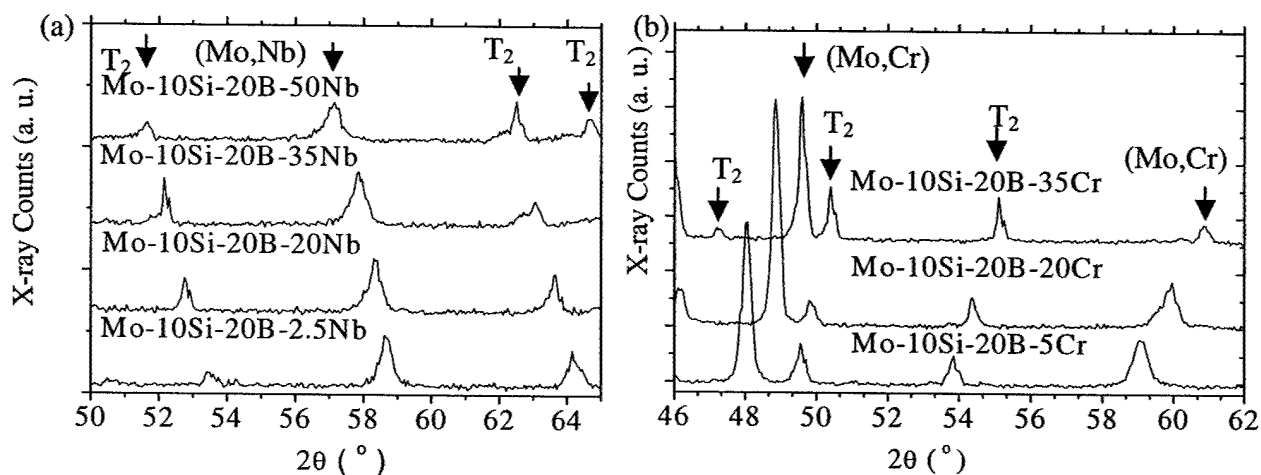
Figure 14 a) XRD data from Mo-Si-B alloys with a)Nb substitution and b) Cr substitution, showing the continuous shift in the peak positions of T_2 as well as Mo(ss) phase as the amount of either Nb or Cr increases.
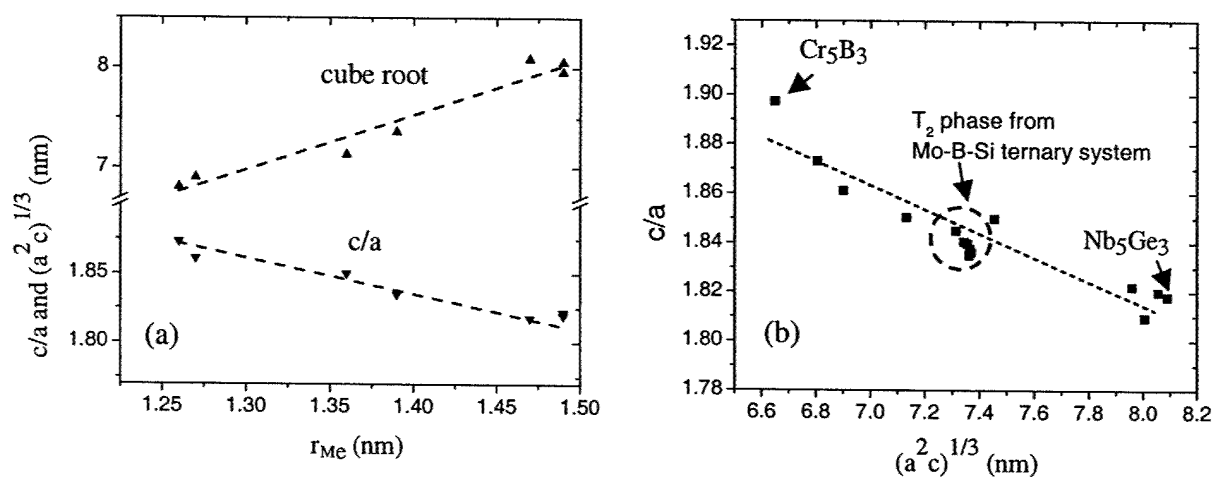
Figure 15 Plot indicating the correlation between r_{Me} the metal atom radius in Me_5SiB_2 (T_2) phases and c/a and $(a^2c)^{1/3}$, (b) Plot showing the correlation between c/a and $(a^2c)^{1/3}$ for transition-metal based T_2 phases.
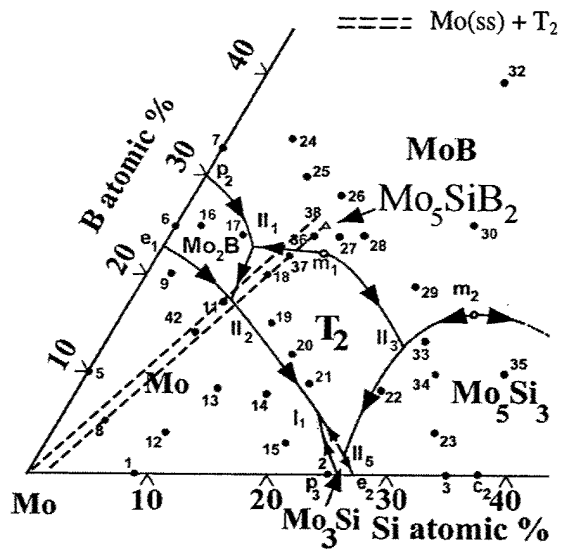
Figure 16 The liquidus projection in the Mo-rich portion of the Mo-Si-B system
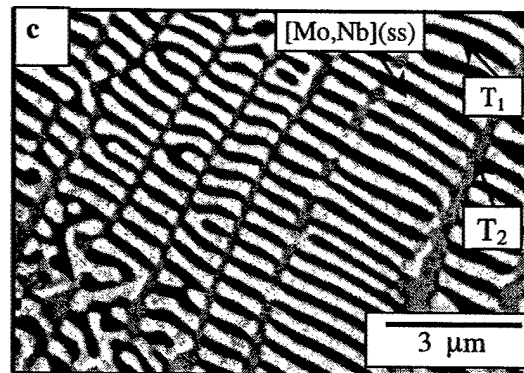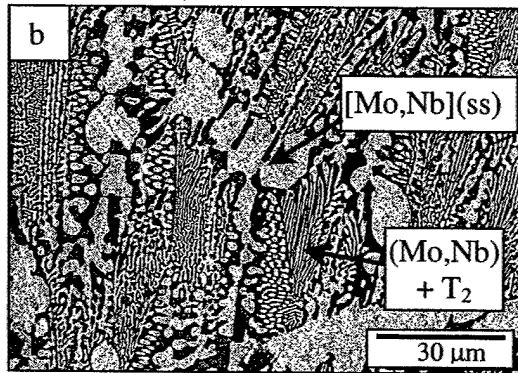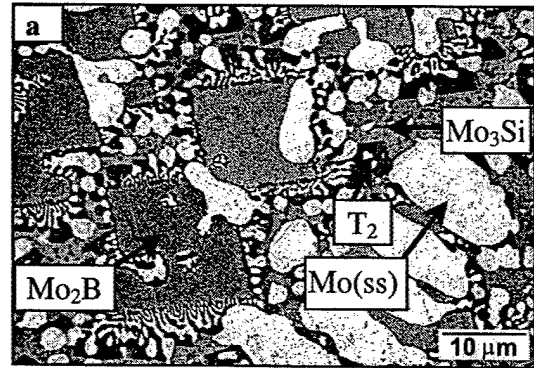
Figure 17. (a) BSE image of as-cast Mo-7Si-14B (alloy # 42) (b) BSE image of as-cast Mo-7Si-14B-5Nb (d) as-cast Mo-7Si-14B –20Nb (b) the three-phase [Mo,Nb](ss) + T_2 + T_1 eutectic
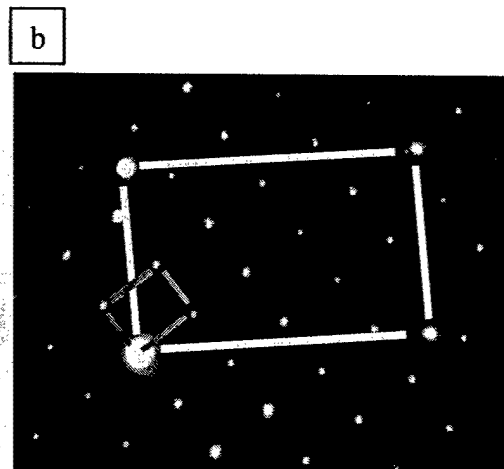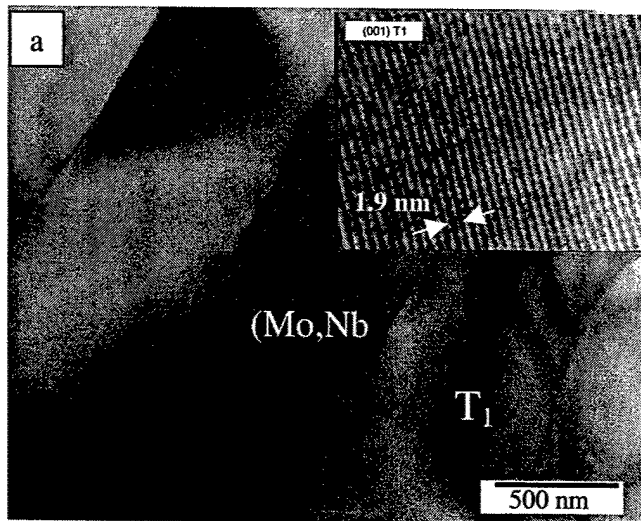

Figure 18 a) Bright-field TEM image of (Mo,Nb) + T_1 eutectic with HR-TEM image of (001) in the inset. b) Crystallographic relations between (Mo,Nb) BCC and T1 phase : $(001)_{T1}//(110)_{BCC}$, $[210]_{T1}//[011]_{BCC}$
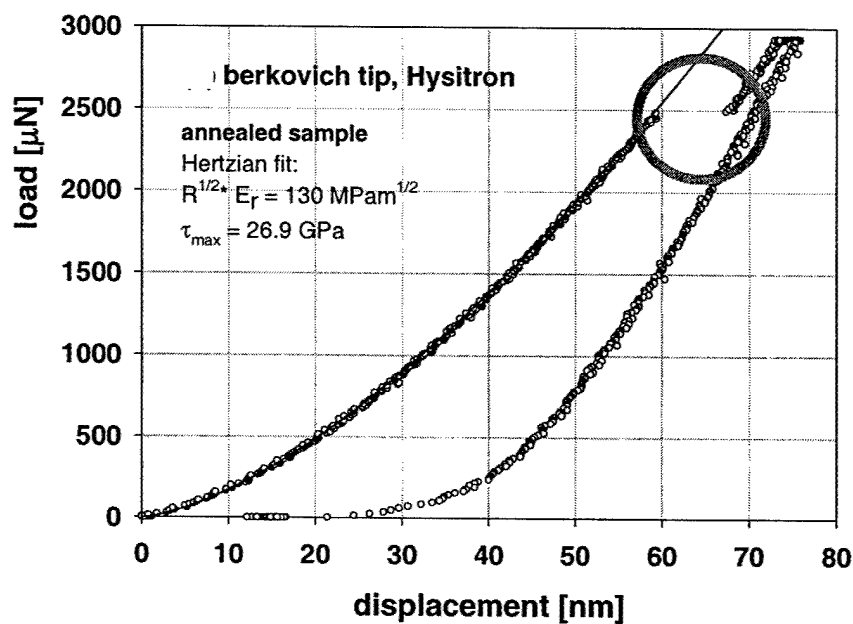
Figure 19 Typical load displacement curves obtained with indents in T_2 phase using Hysitron instruments and berkovich tip. The 'pop-in' phenomenon (circled) was observed during the loading process indicating the initiation of yielding and plasticity as room temperature.
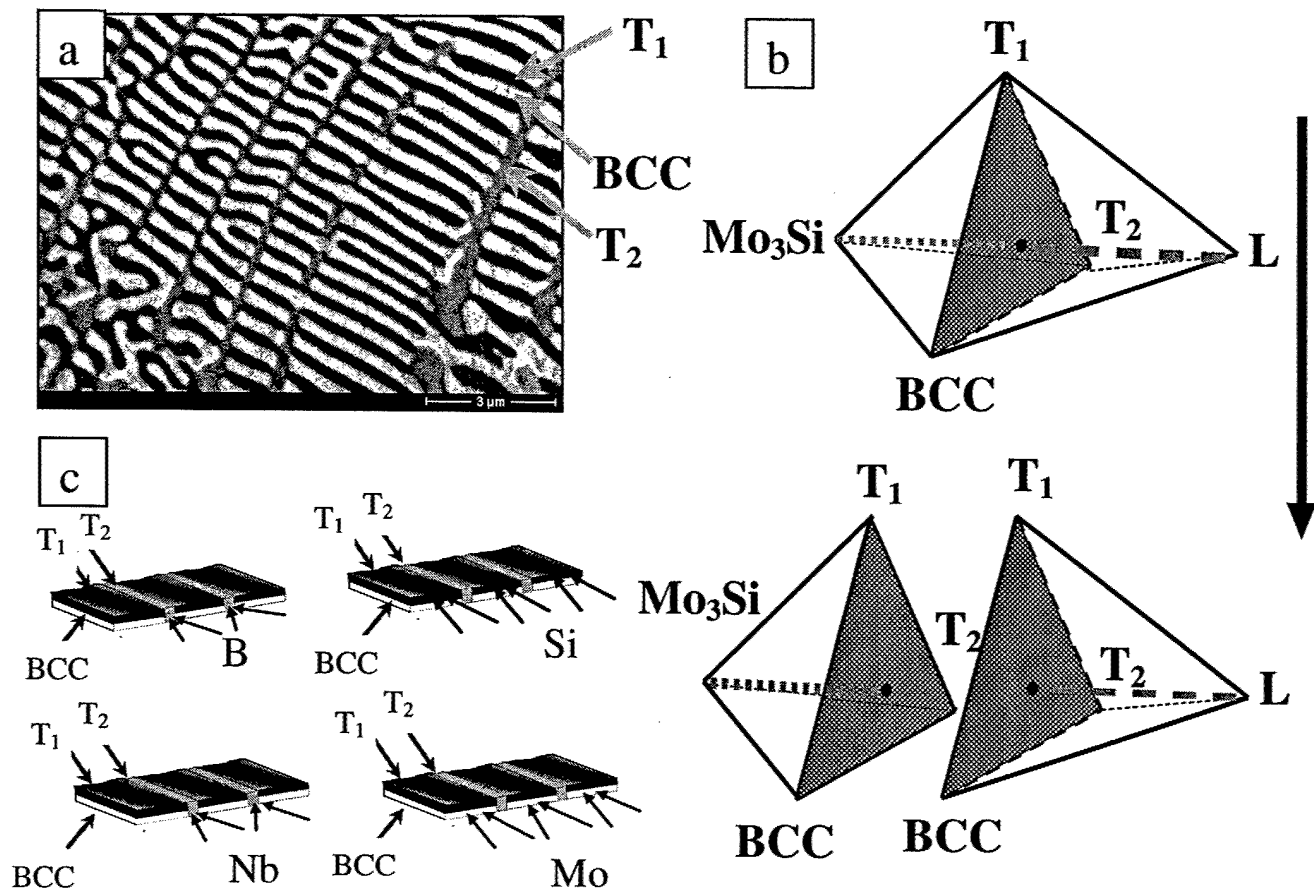
Figure 20 a) BS-SEM image of the BCC + T_2 + T_1 three-phase eutectic, b) Schematic of invariant reaction of $(Mo,RM)_3Si + L \Leftrightarrow BCC + T_2 + T_1$, c) Schematic of the preferential solute partitioning in the growth of the three-phase eutectic
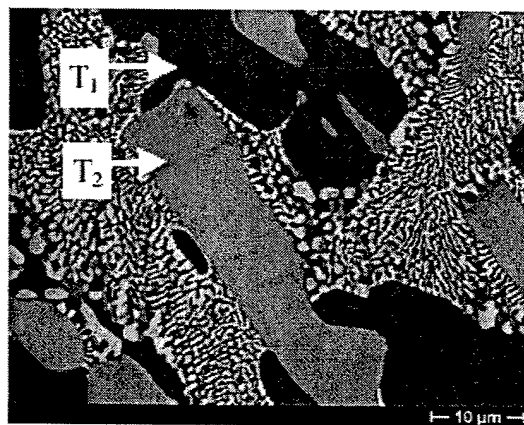

Figure 21. BSE image of Mo-7.5W-23Si-8.9B alloys with the T_2 + T_1 co-primary phases surrounded by the BCC + T_2 + T_1 eutectic